EPJ Web of Conferences **380**, 01004 (2026) https://doi.org/10.1051/epjconf/202638001004
ICISCT'25

Tunable Electromagnetic Response of SRR-Based Metamaterials: A Parametric Study in the X-Band

Ayoub Dafir[1,*], *Lahcen* Ait Benali[2], *Jaouad* Terhzaz[2], *Abdelwahed* Tribak[1], and *Onyonkiton Theophile* Aballo[3]

[1]Institut National des Postes et Télécommunications (INPT), Rabat, Morocco.
[2]Centre Régional des Métiers de l'Éducation et de la Formation Casablanca-Settat (CRMEF CS), Casablanca, Morocco
[3]LETIA/EPAC/UAC University of Abomey-Calavi, Abomey-Calavi, Republic of Benin

Abstract. This study focuses on numerical analysis of a metamaterial based on a Split Ring Resonator (SRR), using wave-based electromagnetic modeling conducted in CST Studio Suite and validated using HFSS. To characterize the magnetic response of the structure, we apply a Lorentz model to the real and imaginary parts of the extracted relative permeability, enabling the estimation of key parameters such as the resonance frequency, damping factor, and magnetic susceptibility.
We further investigate the influence of SRR geometric variations—specifically substrate thickness, gap size, and ring width—on the electromagnetic response. Simulation results reveal that reducing substrate thickness and gap size enhances the resonance strength, leading to deeper dips in the transmission coefficient (S_{21}) and more pronounced negative permeability. Increasing the ring width causes a slight shift in the resonance and affects the quality factor. These findings provide valuable design guidelines for engineering tunable metamaterials based on SRR structures.

1 Introduction

Metamaterials are artificially engineered materials that derive their electromagnetic properties from sub-wavelength structural configurations rather than their intrinsic composition [1]. By tailoring periodic arrangements of resonant unit cells—such as split-ring resonators (SRRs)—these materials exhibit exotic responses, including negative refractive index, perfect lensing, and cloaking [2]. Their homogenized effective parameters (permittivity ε_{eff}, permeability μ_{eff}), and refractive index (n_{eff}) are governed by the geometry and coupling dynamics of individual elements, enabling precise control over wave propagation at designated frequency bands.

Among metamaterial unit cells, the SRR has emerged as a canonical structure for achieving magnetic resonance, with its inductive-capacitive (LC) behavior yielding a frequency-dependent μ_{eff} that can become negative. While the foundational principles of SRRs are well-established [3],

[*]e-mail: dafir.ayoub@gmail.com

The sensitivity of their electromagnetic response to geometric and material parameter variations-such as ring width, substrate thickness, and rings Gap remains critical for optimizing real-world applications, including filters, sensors, and antennas [4].

In this work, we systematically investigate the impact of SRR parameter variations (thickness, ring width, ring gap) on scattering parameters (S_{11}, S_{21}), and real part of permeability. Through CST studio simulation, we quantify how these adjustments influence resonance frequency, resonance coupling. Our results provide actionable design guidelines for designing SRR-based metamaterials to specific application.

2 Cell Design

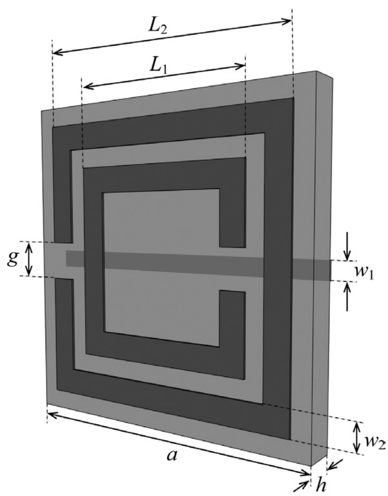

Figure 1. Unit cell of a split ring resonator (SRR)

Figure 1 illustrates the designed double split-ring resonator (SRR) unit cell. The structure consists of an FR-4 dielectric substrate, with a metallic strip on the back and a double square split-ring resonator on the front. The metallic wire primarily induce an effective negative permittivity response, whereas the split-ring resonator is responsible for generating negative permeability.

The geometrical parameters are tuned so that both effective parameters become negative within the same frequency band, providing a left-handed electromagnetic response characterized by a negative refractive index. The detailed geometrical dimensions and material characteristics are summarized in Table 1.
Substrate is FR-4 with a dielectric constant $\varepsilon_r = 4.4$ and loss tangent $\tan\delta = 0.02$.
The metal is considered as copper with thickness t.

3 Theory

3.1 Theoretical s-parameters

Consider a layer of DNG metamaterial composed of the unit cell shown in Fig.1 with a thickness denoted by L . L_0 refer to the distance to the plane of measurement .

Table 1. Geometrical dimensions of the proposed structure.

Parameters	Value (mm)
a	2.5
h	0.25
w_1	0.25
w_2	0.2
L_1	1.5
L_2	2.2
g	0.3
t	0.017

Analytical expressions for the reflection and transmission coefficients were established for a normally incident wave propagating in a waveguide and encountering a DNG layer.

The S-parameters are given by [5, 6]:

$$S_{11} = e^{-2j\mu k_0 L_0} \frac{j((\mu.k_0)^2 - k^2)\sin(kL)}{2\mu k_0 k\cos(kL) + j(\mu k_0^2 + k^2)\sin(kl)} \tag{1}$$

$$S_{21} = \frac{e^{-2j\mu k_0 L_0} 2\mu k_0 k}{2\mu k_0 k\cos(kL) + j((\mu k_0)^2 + k^2)\sin(kl)} \tag{2}$$

Where

$$k_0 = \sqrt{\left(\frac{2\pi f}{c}\right)^2 - \left(\frac{\pi}{a}\right)^2}$$

k_0 : Is the propagation constant in vacuum.

$$k = \sqrt{\varepsilon\mu\left(\frac{2\pi f}{c}\right)^2 - \left(\frac{\pi}{a}\right)^2}$$

k : Is the propagation constant in the slab.
a : Represent the dimensions of the slab.
c : Speed of light in vacuum.

3.2 Theoretical retrieval equations

As it has been pointed out in [7], the refractive index n and the impedance z are obtained by inverting Eqs. 1 and 2, yielding

$$z = \pm\sqrt{\frac{(1+S_{11})^2 - S_{21}^2}{(1-S_{11})^2 - S_{21}^2}} \tag{3}$$

$$e^{jnk_0 d} = X \pm i\sqrt{1 - X^2} \tag{4}$$

Where $X = \frac{1}{2S_{21}}(1 - S_{11}^2 + S_{21}^2)$.
For a passive medium, the sines in Eqs. 3 and 4 are determined by the following requirements:

$$\mathcal{R}(z) \geq 0$$

$$\mathcal{I}m(n) \leq 0$$

Where $\mathcal{R}(.)$ and $\mathcal{I}m(.)$ represent the real and the imaginary part of a complex quantity. The value of the refractive index is given by the equation :

$$n = \frac{1}{k_0 d}\left(\left(\ln(e^{jnk_0 d}) + 2m\pi\right) - j\ln(e^{ink_0 d})\right) \tag{5}$$

Where m refers to an integer that define the branch index of $\mathcal{R}(n)$. It is known that for a homogenized MM slab, its z and $\mathcal{I}m(n)$ can be uniquely extracted from S-parameter measurements [7] without considering the m value.

Finally, ε_r and μ_r are computed from :

$$\varepsilon = n/z \tag{6}$$

$$\mu = nz \tag{7}$$

3.3 Lorentz model

Materials are commonly characterized by their permittivity and permeability that are frequency dependent ($\varepsilon(\omega)$, $\mu(\omega)$).

Therefore, many material models have been developed in order to describe the frequency response of materials (Debye, Drude, Lorentz,...)[8].

Lorentz model is usually presented through two complementary descriptions: the first describes electron motion as a driven, damped harmonic oscillator, while the second characterizes the temporal response of the polarization field:

$$\frac{d^2 P_i}{dt^2} + \Gamma_L \frac{dP_i}{dt} + \omega_0^2 P_i = \varepsilon_0 \chi_L E_i \tag{8}$$

The first term corresponds to the acceleration of the charge, the second refers to the damping, the third represents the restoring forces.
The response :

$$P_i(\omega) = \frac{\chi_L}{-\omega^2 + j\Gamma_L\omega + \omega_0^2}\varepsilon_0 E_i(\omega) \tag{9}$$

The polarization and electric field are linked through the electric susceptibility as follows:

$$\chi_{e,lorentz}(\omega) = \frac{P_i}{\varepsilon_0 E_i(\omega)} = \frac{\chi_L}{-\omega^2 + j\Gamma_L\omega + \omega_0^2} \tag{10}$$

The permittivity can thus be expressed as:

$$\varepsilon_{Lorentz}(\omega) = \varepsilon_0[1 + \chi_{e,lorentz}(\omega)] \tag{11}$$

Similar logic to describe the magnetic response. The permeability can be expressed as follows:

$$\mu_{Lorentz}(\omega) = \mu_0[1 + \chi_{m,lorentz}(\omega)] \tag{12}$$

With :

$$\chi_{m,lorentz}(\omega) = \frac{\chi_{L,m}}{-\omega^2 + j\Gamma_{L,m}\omega + \omega_{0,m}^2} \tag{13}$$

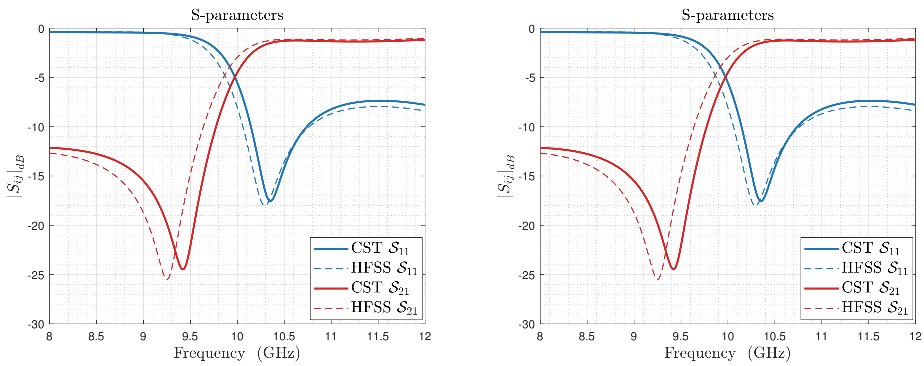

Figure 2. HFSS and CST simulation of S-parameter magnitudes and phases: $|S_{11}|_{dB}$, $|S_{21}|_{dB}$

4 Numerical Results and discussion

4.1 Scattering parameters

Figure 2 compares the complex S-parameters of the SRR unit cell computed with two independent full-wave solvers: CST Studio Suite (finite-integration technique, time-domain solver) and Ansys HFSS (finite-element method, frequency-domain solver). Over the entire 8–12 GHz band, both the magnitude and the phase of S_{11} and S_{21} obtained from the two solvers are in close agreement. Since the two tools rely on different spatial discretizations and different governing formulations, this concordance constitutes a mutual cross-validation of the numerical models.

A deep transmission minimum is observed near 9.4 GHz ($|S_{21}| \approx -25$ dB), identifying the magnetic resonance of the SRR and its associated stop-band response. A reflection minimum occurs near 10.3 GHz, where impedance matching improves and transmission recovers. The phase responses display the expected resonant dispersion, with excellent agreement between CST and HFSS simulations.

Minor discrepancies are observed, with HFSS predicting a slightly lower resonance frequency (by $\sim$ 100–150 MHz) and a deeper transmission minimum than CST. These differences are consistent with the distinct spatial discretizations (hexahedral Finite Integration Technique (FIT) mesh, versus tetrahedral Finite Element Method (FEM) mesh) of the solvers

4.2 Permittivity and permeability

The effective permittivity and permeability of the proposed double SRR metamaterial were retrieved using CST Microwave Studio. As illustrated in Fig.3 and Fig.4, the real part of the relative permittivity ($\mathcal{R}e(\varepsilon_r)$) shows negative values over a broad frequency range. Similarly, the real part of permeability ($\mathcal{R}e(\mu)$) shows a pronounced resonance with a sharp dip that reaches negative values, confirming the double-negative (left-handed) behavior of the structure.

To better understand the shape of the magnetic response, the real and imaginary parts of the relative permeability were modeled using the Lorentz model, as defined by equations (11) and (12). From this model, we extracted key parameters such as the magnetic susceptibility constant $\chi_{L,m}$, the resonance frequency f_r, and the Q-factor . These parameters allowed us to directly determine the damping factor $\Gamma_{L,m}$ and further characterize the resonance behavior.

The extracted values are summarized as follows:

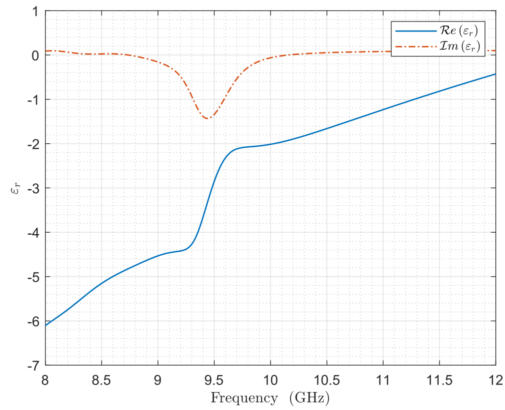

Figure 3. Real and imaginary part relative permittivity

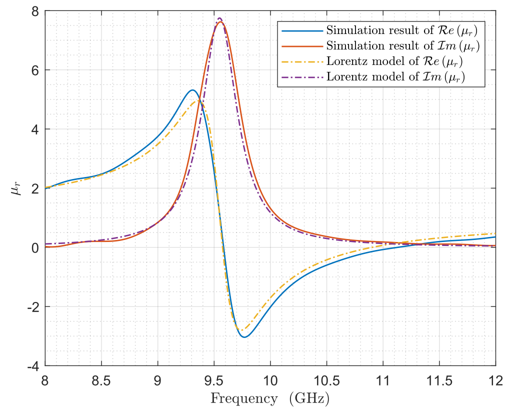

Figure 4. Real and Imaginary Parts of Relative Permeability: CST Simulation vs. Lorentz Model

- Resonance frequency : $f_r = 9.55$ GHz
- Q-factor : $Q = 25$
- Susceptibility constant : $\chi_{L,m} = 0.31$
- Angular frequency : $\omega_{0,m} = 2\pi f_r = 6.10^{10}\text{rad.s}^{-1}$
- damping factor : $\Gamma_{L,m} = \dfrac{2\pi f_r}{Q} = 2.4.10^{9}\text{rad.s}^{-1}$

4.3 refractive index-impedance

The impedance and refractive index of the of the proposed double SRR metamaterial were extracted using CST The results are presented in Fig.5 and Fig.6. We notice a negative refractive index in all the simulated band.

The effective refractive index and wave impedance were extracted from the simulated scattering parameters using the Nicolson–Ross–Weir (NRW) retrieval technique [9, 10]. Both quantities exhibit a pronounced resonant behavior centered near 9.5 GHz, corresponding to the frequency at which the transmission coefficient ($|S_{21}|$) reaches its minimum. This correspondence indicates that the retrieved effective parameters are directly associated with the magnetic resonance induced by the split-ring resonator. Overall, the extracted parameters provide a physically meaningful effective-medium description of the resonant behavior of the unit cell.

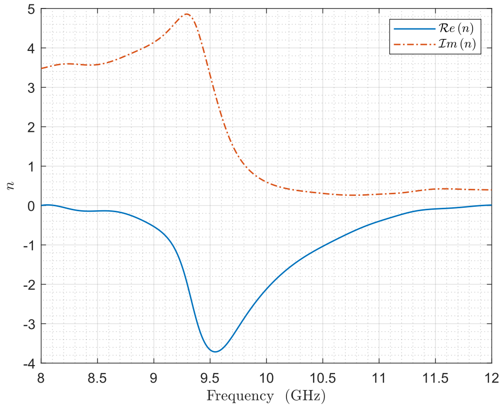

Figure 5. Real and imaginary part of refractive index

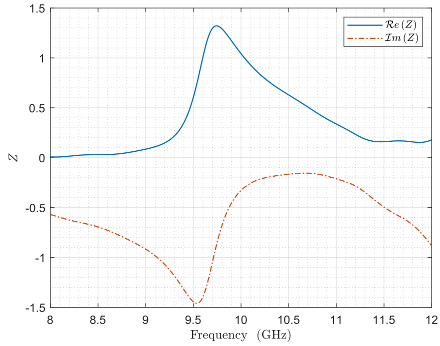

Figure 6. Real and imaginary part of impedance

4.4 Gap Effect

We tested three SRR gap effect ($g = 0.1,\ 0.2,\ 0.3\ mm$). The results are presented in Fig.7 and 8.

As the gap decreases over the range 0.3 mm-0.1 mm the resonance frequency shifts toward lower frequencies (leftward shift of the dip). We also observe no effect on the depth of the dip, by this perturbation.

So the gap tunes the resonance frequency, without affecting the the coupling between the magnetic field and the split ring. We can interpret this effect, smaller the gap induce higher capacitance in the SRR, causes decrease of resonance frequency knowing that it is given by $f_r = \dfrac{1}{\sqrt{LC}}$.

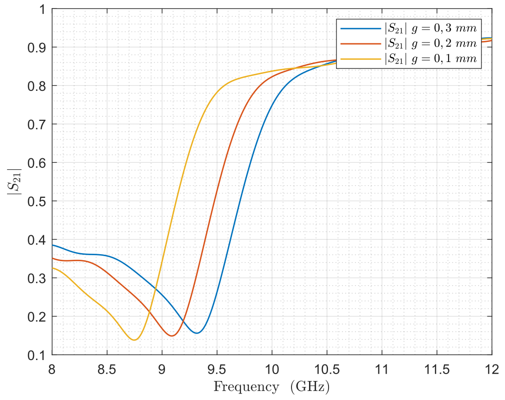

Figure 7. Effect of SRR gap on S_{21} magnitude

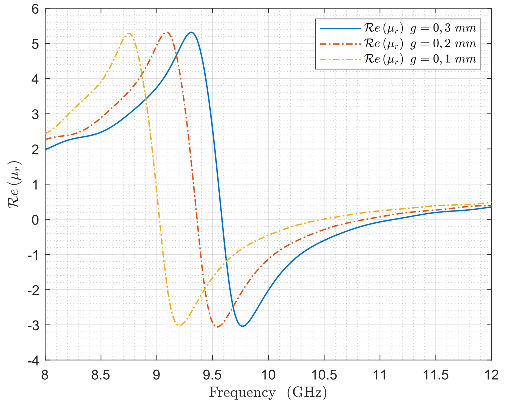

Figure 8. Effect of SRR gap on real part of relative permeability

4.5 Ring Width effect

The plot of S_{21} magnitude vs frequency is presented (Fig9.) for three different SRR ring widths (w = 0.1, 0.2, 0.3 mm) . As the ring width increases, the resonant frequency slightly shifts,and the depth of the dip (resonance strength) changes.

Wider rings (larger w_2) reduce inductance,this can increase the resonant frequency slightly. May weaken the resonance due to increased surface area and possibly higher losses. This result is confirmed by the resonance of permeability Fig.10.

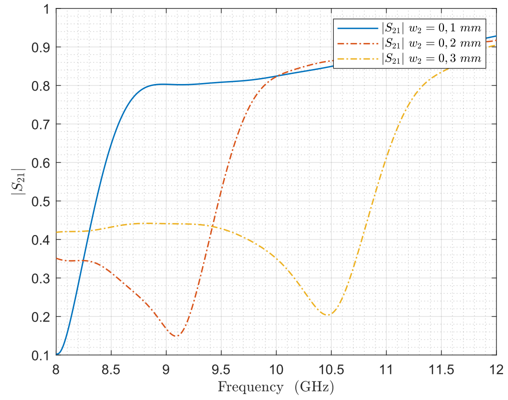

Figure 9. impact of the ring width on the S_{21} magnitude

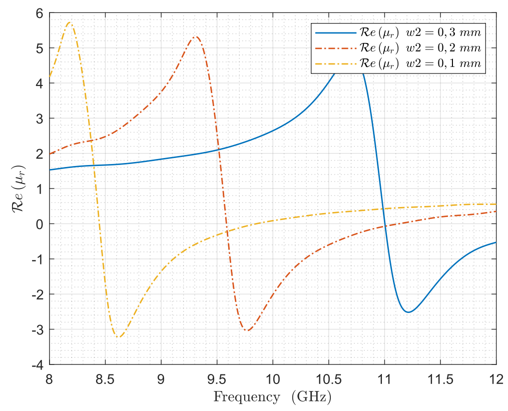

Figure 10. impact of the ring width on the real part of relative permeability

4.6 Slab thickness effect

We tested three SRR thicknesses ($h = 0.5mm,\ 0.8mm,\ 1.6mm$). The results are presented in Fig.11. and Fig.12.

All thicknesses show a transmission dip (S_{21}) at 9.2GHz, confirming magnetic resonance.

Thinner SRRs ($h = 0.5\ mm$) exhibit a deeper S_{21} dip (0.36 or -13 dB vs. 0.26 or -8 dB for $h = 1.6mm$). That can be explained by the fact that thinner the substrate confines the fields closer to the SRR plane, enhancing a stronger coupling. And that can also explain a stronger dip near resonant frequency. This observation can confirmed by the permeability curve (Fig. 12) the fact that the resonance becomes weaker (shallower and broader) as thickness h increases.

V. Conclusion

This study begins by characterizing the magnetic response of a split ring resonator (SRR)-based metamaterial using the Lorentz model. By fitting the real and imaginary parts of the

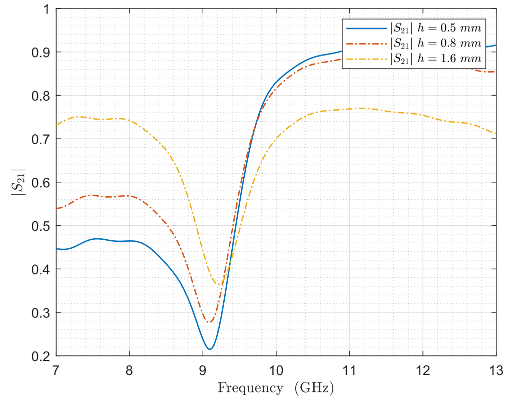

Figure 11. Impact of slab thickness on S_{21} magnitude

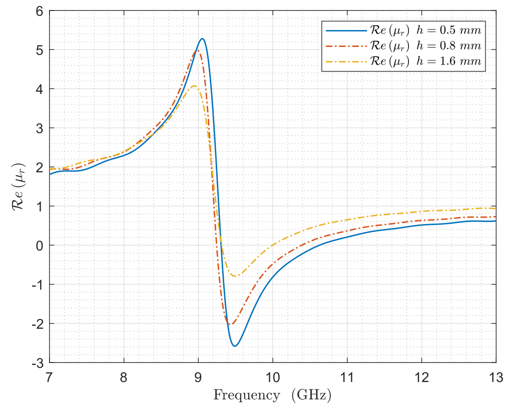

Figure 12. Impact of slab thickness on real part of permeability

extracted relative permeability, we determined key parameters such as the resonance frequency, damping factor, and magnetic susceptibility. Building on this model, we investigated how key geometric parameters-namely substrate thickness, gap size, and ring width-effect the electromagnetic behavior of the SRR. Simulations show that thinner substrates and narrower gaps enhance capacitive and magnetic coupling, resulting in lower resonant frequencies, deeper S_{21} dips, and stronger negative permeability. Conversely, increasing the ring width causes a slight frequency shift and a reduction in resonance strength due to increased conductive losses. These findings underline the importance of combining analytical modeling with geometric optimization in the design of tunable and high-performance metamaterials for advanced electromagnetic applications.

References

1. W. Cai, V.M. Shalaev, *Optical Metamaterials: Fundamentals and Applications* (Springer, New York, 2010). https://doi.org/10.1007/978-1-4419-1151-3
2. F. Capolino (Ed.), *Theory and Phenomena of Metamaterials* (CRC Press, Boca Raton, FL, 2009). https://doi.org/10.1201/9781420054262

3. D.R. Smith, D.C. Vier, T. Koschny, C.M. Soukoulis, Electromagnetic parameter retrieval from inhomogeneous metamaterials. Phys. Rev. E **71**, 036617 (2005). https://doi.org/10.1103/PhysRevE.71.036617
4. M.N. Hamza, M.T. Islam, S. Koziel, Advanced sensor for non-invasive breast cancer and brain cancer diagnosis using antenna array with metamaterial-based AMC. Eng. Sci. Technol. Int. J. **56**, 101779 (2024). https://doi.org/10.1016/j.jestch.2024.101779
5. L. Ait Benali, A. Tribak, J. Terhzaz, T. Fernandez Ibanez, New FDTD method to estimate the dielectric constant and loss tangent of a bilayer dielectric material at X-band frequencies. Int. J. Microw. Opt. Technol. **18**, 575–582 (2023).
6. A. Dafir, L. Ait Benali, J. Terhzaz, A. Tribak, Characterization of metamaterial using K-band rectangular waveguide for 5G applications, in *Proc. 4th Int. Conf. on Innovative Research in Applied Science, Engineering and Technology (IRASET)* (Fez, Morocco, 2024), pp. 1–4. https://doi.org/10.1109/IRASET60544.2024.10548043
7. X. Chen, T.M. Grzegorczyk, B.-I. Wu, J. Pacheco, J.A. Kong, Robust method to retrieve the constitutive effective parameters of metamaterials. Phys. Rev. E **70**, 016608 (2004). https://doi.org/10.1103/PhysRevE.70.016608
8. N. Engheta, R.W. Ziolkowski (Eds.), *Metamaterials: Physics and Engineering Explorations* (Wiley–IEEE Press, Hoboken, NJ, 2006). https://doi.org/10.1002/0471784192
9. A.M. Nicolson, G.F. Ross, Measurement of the intrinsic properties of materials by time-domain techniques. IEEE Trans. Instrum. Meas. **19**, 377–382 (1970). https://doi.org/10.1109/TIM.1970.4313932
10. W.B. Weir, Automatic measurement of complex dielectric constant and permeability at microwave frequencies. Proc. IEEE **62**, 33–36 (1974). https://doi.org/10.1109/PROC.1974.9382